Journal of Magnetic Resonance **139,** 98–108 (1999)
Article ID jmre.1999.1773, available online at http://www.idealibrary.com on IDEAL®

Examples of Hartmann–Hahn Match Conditions for CP/MAS between Two Half-Integer Quadrupolar Nuclei

Margaret A. Eastman

Department of Chemistry, Oklahoma State University, Stillwater, Oklahoma 74078-0447

Received October 2, 1998; revised March 18, 1999

Hartmann–Hahn match conditions for $\frac{n}{2} \rightarrow \frac{m}{2}$ CP/MAS between two quadrupolar nuclei, spin-lock signal as a function of effective nutation frequency, and the correlation of effective nutation frequency and radio-frequency field strength are reported for three samples: sodium diborate ($Na_2B_4O_7$), aluminum boride (AlB_2), and lithium aluminate ($LiAlO_2$). Radiofrequency field strengths used for CP/MAS are both greater and less than the sample spinning speed of 10 kHz, resulting in the observation of both zero-quantum and double-quantum matches, which have signals of opposite sign. The match conditions for $Na_2B_4O_7$ are as expected from published theory and CP/MAS experiments on spins $\frac{1}{2}$ and $\frac{n}{2}$ ($n = 3$ or 5) with quadrupole frequencies (ω_Q) large compared to the radiofrequency field strength of the CP contact pulse, consisting mainly of sideband matches at one and two times the sample spinning frequency, and the correlation of effective nutation frequency and radio-frequency field strength supports the conclusion that ω_Q is large for both ^{11}B and ^{23}Na. Aluminum-27 in AlB_2 may have either small or intermediate ω_Q, and ^7Li in $LiAlO_2$ is proposed to have intermediate ω_Q in relation to the radiofrequency field strength, and both have curves of the spin-lock signal as a function of effective nutation frequency with central minima, differing from those of the nuclei with large ω_Q. The sign of the CP/MAS signal for AlB_2 and $LiAlO_2$ appears to vary with the CP field strengths for the two nuclei so that positive or negative signals cannot be consistently correlated with zero- or double-quantum matches. However, it is possible to assign at least some of the matches as close to integral multiples of the sample spinning frequency, and some of these are matches at greater than two times the sample spinning frequency.

Key Words: **quadrupole; CP/MAS; spin lock; Hartmann–Hahn; double quantum.**

INTRODUCTION

Although double-resonance experiments involving two quadrupolar nuclei of half-integral spin are nothing new (*1*), only recently has cross-polarization (CP) with magic-angle spinning (MAS) been applied to this case (*2, 3*). The $\frac{n}{2} \rightarrow \frac{m}{2}$ CP/MAS experiment has some potential for establishing connectivity (*3*), while it is less likely to be useful for signal enhancement as the two nuclei involved may have comparable magnetogyric ratios and relaxation times. The advent of the MQMAS experiment (*4*) and two-dimensional correlation experiments combining it with CP (*5*) makes it possible that such correlation experiments may be done to establish connectivities between quadrupolar nuclei. Therefore, it may be useful to examine the Hartmann–Hahn match conditions and spin-locking behavior for some readily available polycrystalline samples.

Previous work on CP/MAS involving $\frac{n}{2}$ quadrupolar nuclei suggests that low RF powers and fast spinning speeds should be used (*2, 3, 6–8*). The theoretical work of A. Vega on $\frac{1}{2} \rightarrow \frac{3}{2}$ CP/MAS (*8*) is relevant, since it describes the behavior of a spin $\frac{3}{2}$ as the observed nucleus in CP. Vega treats the case in which the quadrupole frequency ($\omega_Q = 3e^2qQ/\hbar 2S(2S - 1)$) is much larger than the CP radiofrequency, ω_{1S}, and identifies three regimes of spinning speed: adiabatic (slow spinning), intermediate, and sudden (fast spinning), recommending the sudden regime as the most practically useful. He gives the Hartmann–Hahn match conditions as

$$\omega_{1I} - \omega_{1S} = \pm n\omega_R, \{n = 1, 2\} \quad \text{for } \omega_Q \ll \omega_{1S}, \quad [1]$$

$$\omega_{1I} = \left(S + \frac{1}{2}\right)\omega_{1S} \quad \text{for the adiabatic regime with } \omega_Q \gg \omega_{1S}, \quad [2]$$

and

$$\omega_{1I} - \left(S + \frac{1}{2}\right)\omega_{1S} = \pm n\omega_R, \{n = 1, 2\} \quad \text{for the sudden regime with } \omega_Q \gg \omega_{1S}, \quad [3]$$

where ω_R is the angular frequency at which the sample is spun. The factor of $S + \frac{1}{2}$ enters in the case of $\omega_Q \gg \omega_{1S}$, because the central transition is excited nearly selectively and it can be treated as a ficticious spin $\frac{1}{2}$ (*9*).

In addition to the above conditions, sum matches are expected that have forms such as

$$\omega_{1I} + \omega_{1S} = n\omega_R \quad \text{for } \omega_Q \ll \omega_{1S}, \quad [4]$$

and

$$\omega_{1I} + \left(S + \frac{1}{2}\right)\omega_{1S} = n\omega_R \quad \text{for } \omega_Q \gg \omega_{1S}. \quad [5]$$

1090-7807/99 $30.00

These or analogous conditions have been found previously for $^{1}H \rightarrow {}^{13}C$ (*10*) and $^{27}Al \rightarrow {}^{29}Si$ (*11*) CP/MAS, and most recently in CP/MAS between two half-integer quadruplar nuclei (*3*). The sum and difference match conditions have been described thermodynamically by Meier (*10*) for CP/MAS involving spins $\frac{1}{2}$. Sum matches are associated with heteronuclear double-quantum transitions and difference matches with heteronuclear zero-quantum transitions; the signals from the two types of match are opposite in sign. This can also be seen using a theoretical formalism like that presented by Stejskal *et al.* (*12*). Since these conditions are due to the heteronuclear dipolar interaction, they will obtain in general for spins other than $\frac{1}{2}$.

The limiting Hartmann–Hahn match conditions given above for very small or very large ω_Q can be seen to arise even though the match conditions depend in general upon the crystallite orientation in a powder sample (*13*). For very large (small) ω_Q, the quadrupole interaction which becomes time dependent with sample spinning will, despite 2 or 4 zero crossings of the first-order quadrupole splitting per rotor period (*8, 14*), be large (small) for most crystallites most of the time, giving a nutation frequency of $(S + \frac{1}{2})\omega_{1S}$ (ω_{1S}). When ω_Q has an intermediate value relative to ω_{1S}, no such approximation can be made and the dependence of the match conditions upon crystallite orientation may result in their being ill-defined and following no simple formula (*8*). In the intermediate case multiple nutation frequencies may be expected (*15, 16*) and separate match conditions for each transition might also occur (*17*).

A reasonable general extension to the $\frac{n}{2} \rightarrow \frac{m}{2}$ case of the match conditions given above are the difference and sum forms

$$\epsilon_I\omega_{1I} - \epsilon_S\omega_{1S} = \pm n\omega_R \qquad [6]$$

and

$$\epsilon_I\omega_{1I} + \epsilon_S\omega_{1S} = n\omega_R, \qquad [7]$$

where ϵ_I (ϵ_S) can take on values from 1 to $I + \frac{1}{2}$ ($S + \frac{1}{2}$) (*2, 15*). As noted, particular conditions of this sort apply to each individual crystallite in a powder, but average matches for the entire sample following this simple form may be expected at least when the ω_Q values are very large or very small. The quantities ω_{1I} and ω_{1S} correspond to radiofrequency field strengths that are appropriately obtained from 90° pulse widths of liquid-state samples (*18*), but the quantities $\epsilon_I\omega_{1I}$ and $\epsilon_S\omega_{1S}$ are nutation frequencies of the solid sample. For a polycrystalline sample under MAS the first maximum in the signal intensity as the pulse width is increased is readily measured, while the exact nutation frequencies for each site in each crystallite are not so easily obtained. We will refer to this pulse width as the solid-state maximum-signal pulse width (pw_M) and associate with it a frequency, ν', called the effective nutation frequency, equal to $1/(4pw_M)$. Correlation of the 90° pulse width for a liquid sample with pw_M for the solid as a function of ω_{1I} provides collective values of ϵ_I representing all crystallites, which should be identifiable as $I + \frac{1}{2}$ and 1 in the cases of very large and very small ω_{QI}, respectively. The Hartmann–Hahn match conditions can be compared to the forms

$$\nu'_I - \nu'_S = \pm n\nu_R \qquad [8]$$

and

$$\nu'_I + \nu'_S = n\nu_R, \qquad [9]$$

where angular frequencies have been replaced by frequencies for convenience and ν_R equals $\omega_R/2\pi$. Deviation from these forms is expected when ω_{QI} or ω_{QS} is intermediate in size relative to the radiofrequency field strength ω_{1I} or ω_{1S}.

Based on the second rank nature of the heteronuclear dipolar interaction (*12, 14*), values of n would be restricted to 1 or 2. However, values of zero and integer values greater than 2 have been observed (*6, 10–12*). In addition to the particular situation of Eq. [2] above explained by Vega (*8*), two explanations for these observations can be found in the literature. First, these higher order matches may be due to homonuclear dipolar interactions, which further separate the matches at n of 1 and 2 into sidebands at multiples of the spinning frequency (*12*). They may also be accounted for by second- or higher order effects of the heteronuclear dipolar interaction (*10, 19*).

The importance of spin locking to effective CP/MAS and the difficulties of achieving adequate spin locking for the central transition of half-integer quadrupolar nuclei, given the time-dependence of the first-order quadrupole interaction under MAS, have been considered by Vega, who found that the adiabatic and sudden regimes are more favorable for spin locking than are intermediate spinning rates (*7*). Subsequently, Sun *et al.* (*20*) showed that even in the sudden regime, central transition coherence decays rapidly when the radiofrequency field strength and the sample rotation frequency are about equal. Jeschke (*21*) has concluded based upon a Floquet formalism using abstract spins that proper spin locking for a spin $\frac{3}{2}$ with large ω_Q requires that the sample spinning frequency be greater than the radiofrequency field strength. All of this work has stresed the regime in which ω_Q is much larger than the radiofrequency field strength.

In this paper, we describe observations on the Hartmann–Hahn match conditions for $\frac{n}{2} \rightarrow \frac{m}{2}$ CP/MAS for three polycrystalline compounds: sodium diborate, aluminum boride, and lithium aluminate. These compounds are promising candidates for the CP technique due to short distances between the quadrupolar nuclei, which are about 0.3 nm or less as determined by X-ray crystallography (*22–24*). Given the considerations mentioned above, we have chosen the fastest readily achievable spinning speed for our apparatus (ν_R = 10 kHz), and radiofrequency field strengths both less than and greater than the spinning speed. In addition to evaluation of the Hartmann–Hahn match conditions in terms of the effective nutation fre-

quencies according to Eqs. [8] and [9], spin-locking experiments are presented, and liquid-state 90° pulse widths are compared with solid-state pw_M values over the range of powers used in the CP/MAS and spin-locking experiments to estimate the size of the quadrupole frequencies. Correlations between the patterns seen in the these three types of experiments are considered.

EXPERIMENTAL

Samples

Sodium diborate ($Na_2B_4O_7$) was made by melting borax ($Na_2B_4O_7 \cdot 10H_2O$) at 800°C, using the procedure of Krogh-Moe (*22*). Aluminum boride (AlB_2) and lithium aluminate (γ-$LiAlO_2$) were used as obtained from Alfa Æsar.

NMR Experiments

Experiments were performed on a Chemagnetics CMX-II spectrometer operating at 301.0 MHz for ^{1}H, with a Chemagnetics triple resonance (H–X–Y) Pencil-II-type magic-angle spinning probe. The sample spinning speed was 10.00 ± 0.05 kHz for all experiments on solid samples in which the speed was controlled with a Chemagnetics MAS speed controller that regulated only the drive air stream. For some CP/MAS experiments, the speed was controlled to ±0.005 kHz with a newer model Chemagnetics MAS speed controller that regulated both the bearing and the drive air streams. Resonance frequencies for ^{7}Li, ^{11}B, ^{23}Na, and ^{27}Al are given in Table 1 along with the relaxation delay times used for obtaining 90° or pw_M pulse widths and for spin locking for the various samples and the reference used for each nucleus. Delays used in the CP/MAS experiments were 0.5 s for ^{11}B observation and 1.0 s for ^{23}Na observation in sodium diborate, 0.5 s for ^{11}B observation and 1.0 or 4.0 s for ^{27}Al observation in aluminum boride, and 4.0 s for ^{7}Li observation and 20.0 s for ^{27}Al observation in lithium aluminate. These are different in some cases from those in Table 1, since a compromise was sometimes made with the delay times to reduce experiment time. One molar aqueous solutions of Li_2SO_4, NaCl, and $Al(NO_3)_3$ and a saturated aqueous solution of H_3BO_3 were used to obtain liquid-state 90° pulse widths for determination of the radiofrequency field strength. Ninety-degree pulse widths were obtained for the liquid samples as one-half the pulse width giving minimum signal, and pw_M for solid samples was the pulse width giving maximal signal.

TABLE 1
Resonance Frequencies, Reference Samples, and Pulse Delays for Liquid and Solid Samples

Nucleus	Reference (0 ppm)	Sample	Frequency (MHz)	Pulse delay (s)
^{7}Li	1 M $LiNO_3$ (aq.)	1 M Li_2SO_4 (aq.)	116.980	40.0
		$LiAlO_2$	116.980	60.0
^{11}B	H_3BO_3 (sat. aq.)	H_3BO_3 (sat. aq.)	96.575	0.5
		AlB_2	96.572	15.0
		$Na_2B_4O_7$	96.573	4.0
^{23}Na	1 M NaCl (aq.)	1 M NaCl (aq.)	79.620	1.0
		$Na_2B_4O_7$	79.620	0.5
^{27}Al	1 M $Al(NO_3)_3$ (aq.)	1 M $Al(NO_3)_3$ (aq.)	78.431	1.0
		AlB_2	78.560	0.5
		$LiAlO_2$	78.437	10.0

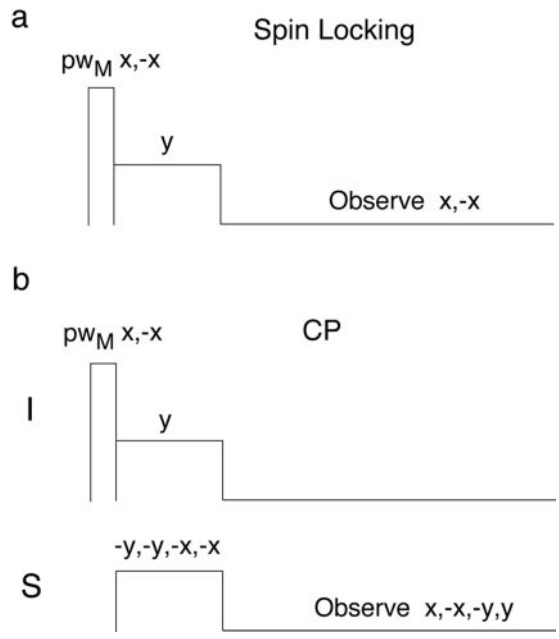

FIG. 1. (a) Pulse sequence used for spin-locking/MAS experiments. (b) Pulse sequence used for CP/MAS experiments. In both a and b pw_M is the (smallest) pulse width giving the maximum signal for the solid sample.

For spin-locking (*7*, *8*) and CP/MAS (*6*, *8*, *25*) experiments the pulse sequences shown in Fig. 1 were used. For spin locking, values of ν' were calculated from solid-state maximum-signal pulse width data taken at the power settings for each spin-lock experiment. In CP experiments the power level of the contact pulse for one of the nuclei was kept constant, while that for the other nucleus was varied in an array to determine the match conditions. Values of ν' were obtained from a fourth-order polynomial equation fitted to ν' values determined from solid-state maximum-signal pulse width data at a subset of power settings in the range used in the CP experiment. Solid-state maximum-signal pulse widths were 3 to 8.5 μs for spin-locking experiments and 3 to 5 μs for CP/MAS experiments, except where indicated in the figure legends. Both X → Y and Y → X experiments were done. Contact times were 2.5 ms for sodium diborate and 1.0 ms for aluminum boride and lithium aluminate; these values were not optimized to give the best possible signal-to-noise ratio.

Signal-to-noise ratios for the CP/MAS spectra were evaluated graphically by measuring the signal and peak-to-peak noise heights on plots with a ruler. To compare signals from different experiments on one sample in which the same nucleus was observed, a relative signal-to-noise ratio was calculated by

dividing the signal-to-noise ratio by the square root of the number of scans taken in the experiment, then normalizing by dividing by the largest value for all spectra in the group of experiments.

RESULTS

Figures 2 and 3 show the results of spin-locking experiments for each nucleus. The integral of the spin-lock signal at a time equivalent to the contact time used in CP/MAS experiments is plotted as a function of the effective nutation frequency for the spin-lock pulse, ν', obtained from the solid-state maximum-signal pulse width. The nuclei fall into two categories based on the appearance of the spin-lock integral curve. ^{11}B in $Na_2B_4O_7$ and AlB_2, ^{23}Na in $Na_2B_4O_7$, and ^{27}Al in $LiAlO_2$ all have a maximum of the integral of the spin-lock signal at ν' values less than 5 kHz, with the integral decreasing as the power is increased. For ^{27}Al in $LiAlO_2$ (Fig. 3a) an additional set of experiments at smaller increments of power shows that the spin-lock signal oscillates as it decreases in magnitude. ^{7}Li in $LiAlO_2$ and ^{27}Al in AlB_2 have a different pattern with a peak at less than 5 kHz, a distinct minimum in the signal with increasing power, followed by a return to high signal levels at the highest powers shown. Again, more detail is given by a separate series of experiments on ^{27}Al in AlB_2 (Fig. 3b), indicating how the signal oscillates as it increases from the central minimum.

Intensity of the spin-lock signal over time (1.0 to 5.0 ms total) was observed, but is not shown. The shapes of the curves vary with the sample, nucleus, and power level. Many of them show a decrease of the signal with time, without oscillations. Some of the nuclei in the first group mentioned above show oscillations in the signal with time that extend out to about 1.0 ms or more at ν' values of less than 2 kHz. Higher frequency oscillations that die out in tenths of a millisecond are sometimes seen in the range of 3–20 kHz for both groups of nuclei.

Figure 4 gives representative CP/MAS spectra for each nucleus in each sample with phases adjusted to make all signals positive, compared with directly detected MAS spectra. Figures 5 through 7 present the results of CP/MAS experiments performed to detect the match conditions, showing the dependence of the integral of the CP signal on ν'. Both zero-quantum and double-quantum matches are evident, as both positive and negative signals occur. A single zero-order phase adjustment was applied to all spectra in an array of CP/MAS experiments; this phase was as close as possible to the phase required for direct detection of the nucleus observed in the CP/MAS experiment, but ensured that all spectral lines were pure absorptive and either positive or negative.

Since the absolute phase of the signals is not known, the assignment of positive and negative signals to sum and difference matches is not determined exactly. For $Na_2B_4O_7$ (Fig. 5), the association of positive signals with sum matches leads to a pattern of matches (Eqs. [8] and [9]) falling exclusively at increments of the spinning frequency of the sample; the opposite assignment is quite different and has no matches at these theoretically favored positions. A weak match peak (not shown) that might correspond to a match at $3\nu_R$ was seen, but

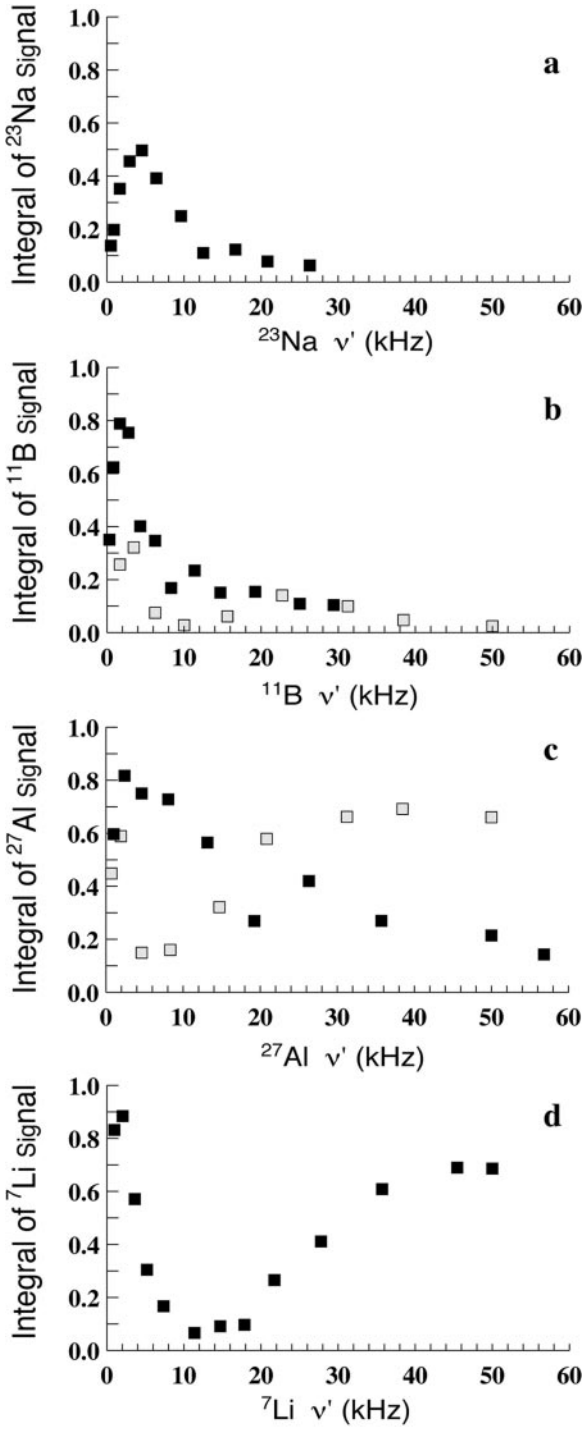

FIG. 2. Results of spin-locking experiments on (a) ^{23}Na in $Na_2B_4O_7$, (b) filled squares, ^{11}B in $Na_2B_4O_7$, stippled squares, ^{11}B in AlB_2, (c) filled squares, ^{27}Al in $LiAlO_2$, stippled squares, ^{27}Al in AlB_2, and (d) ^{7}Li in $LiAlO_2$. Plotted is the integral of the signal at the spin-locking time (2.5 ms for $Na_2B_4O_7$, 1.0 ms for AlB_2 and $LiAlO_2$) normalized by dividing by the integral for a spin-locking time of 0.001 ms. Here and in all subsequent figures the effective nutation frequencies, ν', are calculated from pw_M values of the solid sample.

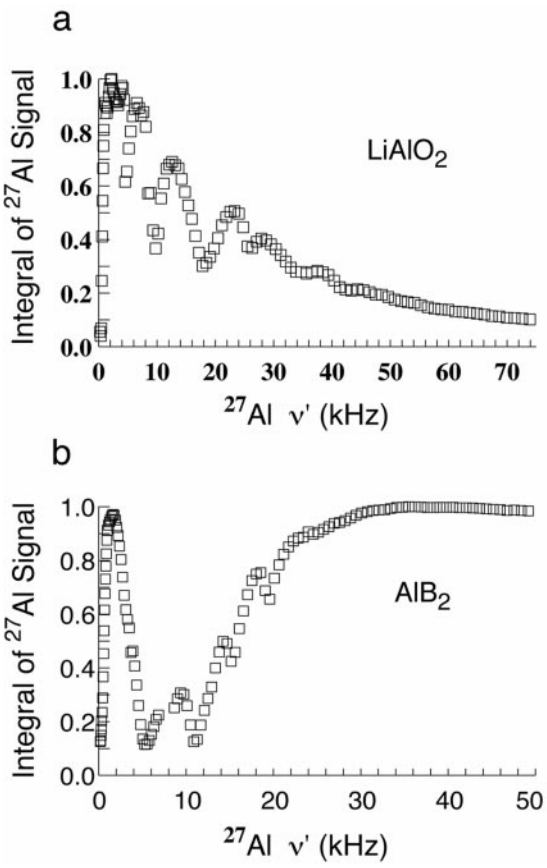

FIG. 3. Integral of the signal at 1.0 ms vs ν' for spin-locking experiments on ^{27}Al in (a) $LiAlO_2$ and (b) AlB_2. Integrals are normalized such that the largest value on each plot is 1 (not relative to a spin-locking time of 0.001 ms as in Fig. 2).

the decrease in signal amplitude in the CP/MAS and spin-locking experiments as the power is increased suggests that strong CP signals would not be found at higher multiples of ν_R.

The assignment of the positive and negative signals for the other compounds is not so simple. For aluminum boride, examination of Figs. 6c and 6d reveals that all the major peaks in these experimental arrays can be assigned to sum or difference matches with n an integer in the range of zero to 4. However, it appears that in Fig. 6c, zero-quantum or difference matches have positive signals, and double-quantum or sum matches have negative signals, whereas in Fig. 6d the opposite assignment of signal signs makes sense. In an additional series of experiments, not shown, the signs of the $^{27}Al \rightarrow {}^{11}B$ (AlB_2) and $^7Li \rightarrow {}^{27}Al$ ($LiAlO_2$) CP/MAS signals changed with ν' for several sets of effective nutation frequencies that should represent $n = 0$ matches and $n = 1$ difference matches. Thus, there is no apparent consistent correlation between signal sign and match type for these compounds. For AlB_2, supposed $n = 1$ difference matches had negative signal if one or both values of ν' were above about 20 kHz and positive signal if both were below about 20 kHz. Consistent with this result, the matches of Fig. 6a are assigned as double-quantum, those of Fig. 6b are double-quantum or have equivalent values of ν' ($n = 0$), and those of Figs. 6c and 6d are assigned as noted above. No readily identifiable pattern could be observed for lithium aluminate that would suggest the assignment of zero-quantum and double-quantum matches. Several prominent matches with sum or difference of the effective nutation frequencies close to an integral multiple of the spinning speed are marked with asterisks in Fig. 7. These had negative signals associated with zero-quantum or difference matches, except the negative signals of Fig. 7c are interpreted as double-quantum or sum matches.

Figure 8 shows plots of the relative signal-to-noise ratio vs the sum (cf. Eq. [9]) or absolute value of the difference (cf. Eq. [8]) of the effective nutation frequencies ν' for the two nuclei, including the major match peaks of Figs. 5–7. Sum and difference matches were assigned as indicated in the last two paragraphs. For $LiAlO_2$ only the peaks marked with asterisks in Fig. 7 are included in Fig. 8c. The relative signal-to-noise ratio should be viewed as a qualitative indicator of the signal strength since peak heights were variable in replicated experiments, as Figs. 6 and 7 suggest. Data from more than one similar or identical array of spectra which appeared to display essentially the same set of match conditions, where available, were averaged together in Fig. 8.

Figure 9 displays the ratio of liquid-state 90° pulse width to solid-state maximum-signal pulse width as a function of the radiofrequency field strength, which is determined from the liquid-state 90° pulse width. The nuclei ^{11}B in $Na_2B_4O_7$ and AlB_2, ^{23}Na in $Na_2B_4O_7$, and ^{27}Al in $LiAlO_2$ all have a liquid-to-solid pulse width ratio of $I + \frac{1}{2}$ over the range of field strengths employed in the CP/MAS experiments, indicating that they are in the regime in which the quadrupole frequency is much greater than ω_{1I}. ^{27}Al in AlB_2 seems to be in the regime of very low ω_Q, and ^7Li in $LiAlO_2$ appears to be in the intermediate region, with the pulse width ratio increasing to about 1.5 with decreasing field strength.

DISCUSSION

The ratio of liquid-state 90° pulse width to solid-state maximum-signal pulse width should be 1 at higher strength where ω_{QI} is much smaller than the field strength ω_{1I}, and $I + \frac{1}{2}$ at lower strength where ω_{QI} is much greater than ω_{1I}. In the intermediate region where ω_{QI} and ω_{1I} are comparable in size, some value between 1 and $I + \frac{1}{2}$ is expected. Some of the trends in Fig. 9 can be interpreted as artifacts; for example, the ratio should not decrease with decreasing field strength. Despite imperfections in the data, conclusions about the size of ω_Q drawn from Fig. 9 are with one exception consistent with published information about the quadrupole frequencies. The quantity e^2qQ/h is generally reported, and this can be translated easily into the form given for ω_Q in the Introduction. Values of $\omega_Q/2\pi$ from the literature are 265 and 320 kHz for ^{11}B and 10.8 kHz for ^{27}Al in AlB_2 (*26*), and 480 kHz for ^{27}Al in γ-$LiAlO_2$ (*27*). These values suggest that ^{11}B in AlB_2 and

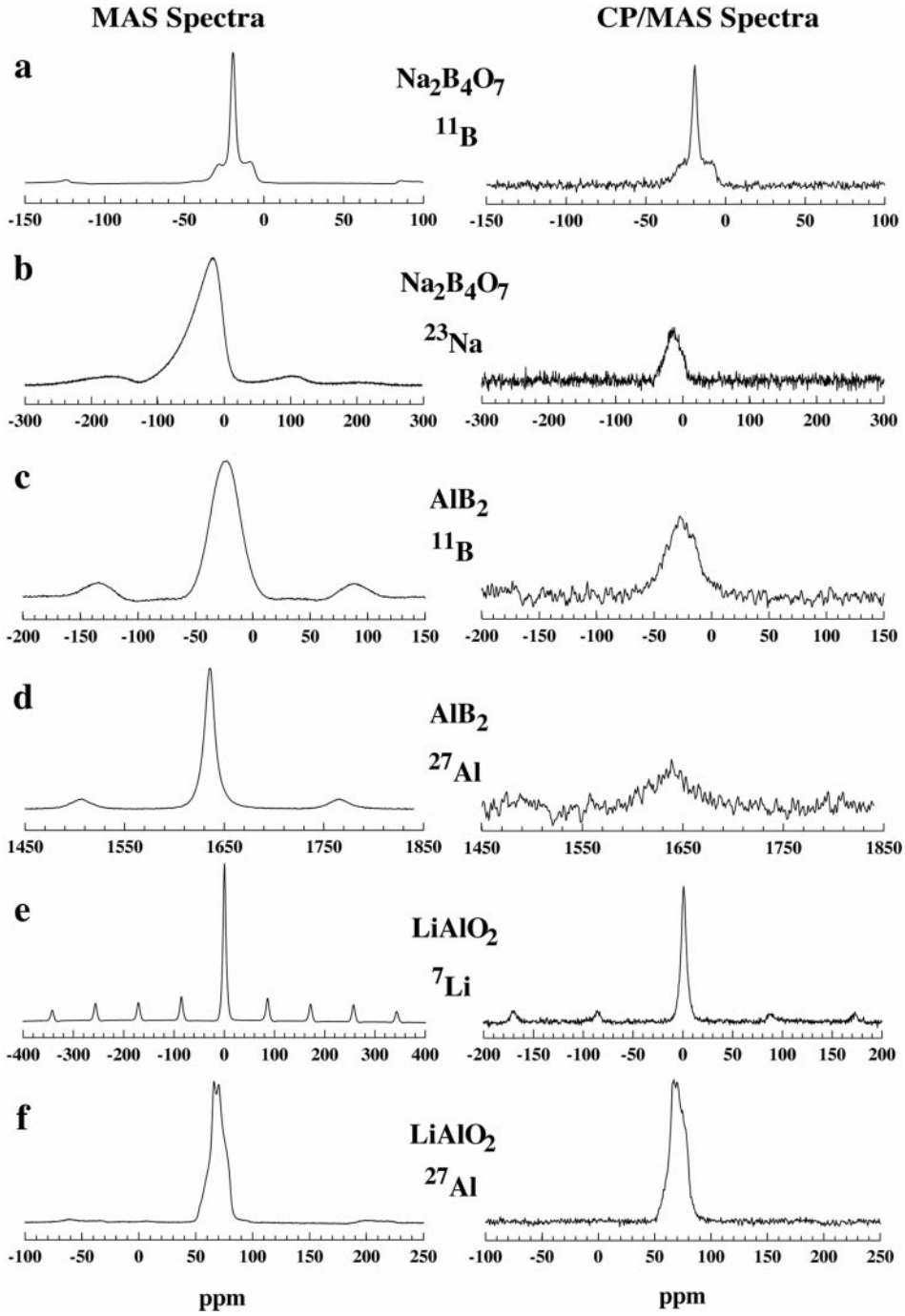

FIG. 4. On the left are directly detected MAS spectra of (a) ^{11}B in $Na_2B_4O_7$, 256 scans, (b) ^{23}Na in $Na_2B_4O_7$, 2048 scans, (c) ^{11}B in AlB_2, 64 scans, (d) ^{27}Al in AlB_2, 256 scans, (e) ^{7}Li in $LiAlO_2$, 16 scans, and (f) ^{27}Al in $LiAlO_2$, 64 scans. Pulse delays are given in Table 1. On the right are X $\rightarrow$ Y CP/MAS spectra. (a) $^{23}Na \rightarrow {}^{11}B$ of $Na_2B_4O_7$, 2048 scans, 0.5 s delay, $\nu'_B = 2.4$ kHz, $\nu'_{Na} = 7.6$ kHz, (b) $^{11}B \rightarrow {}^{23}Na$ of $Na_2B_4O_7$, 1024 scans, 1.0 s delay, $\nu'_B = 7.0$ kHz, $\nu'_{Na} = 2.2$ kHz, (c) $^{27}Al \rightarrow {}^{11}B$ of AlB_2, 4800 scans, 0.5 s delay, $\nu'_B = 3.8$ kHz, $\nu'_{Al} = 6.5$ kHz, (d) $^{11}B \rightarrow {}^{27}Al$ of AlB_2, 4096 scans, 1.0 s delay, $\nu'_B = 3.0$ kHz, $\nu'_{Al} = 6.8$ kHz, (e) $^{27}Al \rightarrow {}^{7}Li$ of $LiAlO_2$, 512 scans, 4.0 s delay, $\nu'_{Li} = 22.7$ kHz, $\nu'_{Al} = 2.2$ kHz, (f) $^{7}Li \rightarrow {}^{27}Al$ of $LiAlO_2$, 64 scans, 20.0 s delay, $\nu'_{Li} = 2.3$ kHz, $\nu'_{Al} = 8.3$ kHz.

^{27}Al in $LiAlO_2$ have large ω_Q relative to the field strength and should have a pulse width ratio of $I + \frac{1}{2}$ in agreement with Fig. 9. The value for ^{27}Al in AlB_2 implies low ω_Q at higher field strengths and intermediate ω_Q at lower field strengths, which is not supported by Fig. 9b. This nucleus is distinguished by a substantial Knight shift (cf. scale in Fig. 4d) which has been reported to have no anisotropy (*26*), and aluminum boride is a metallic conductor (*28*).

Spin-locking experiments in the literature mainly show intensity as a function of spin-lock time (*2, 3, 8, 20, 21*). De

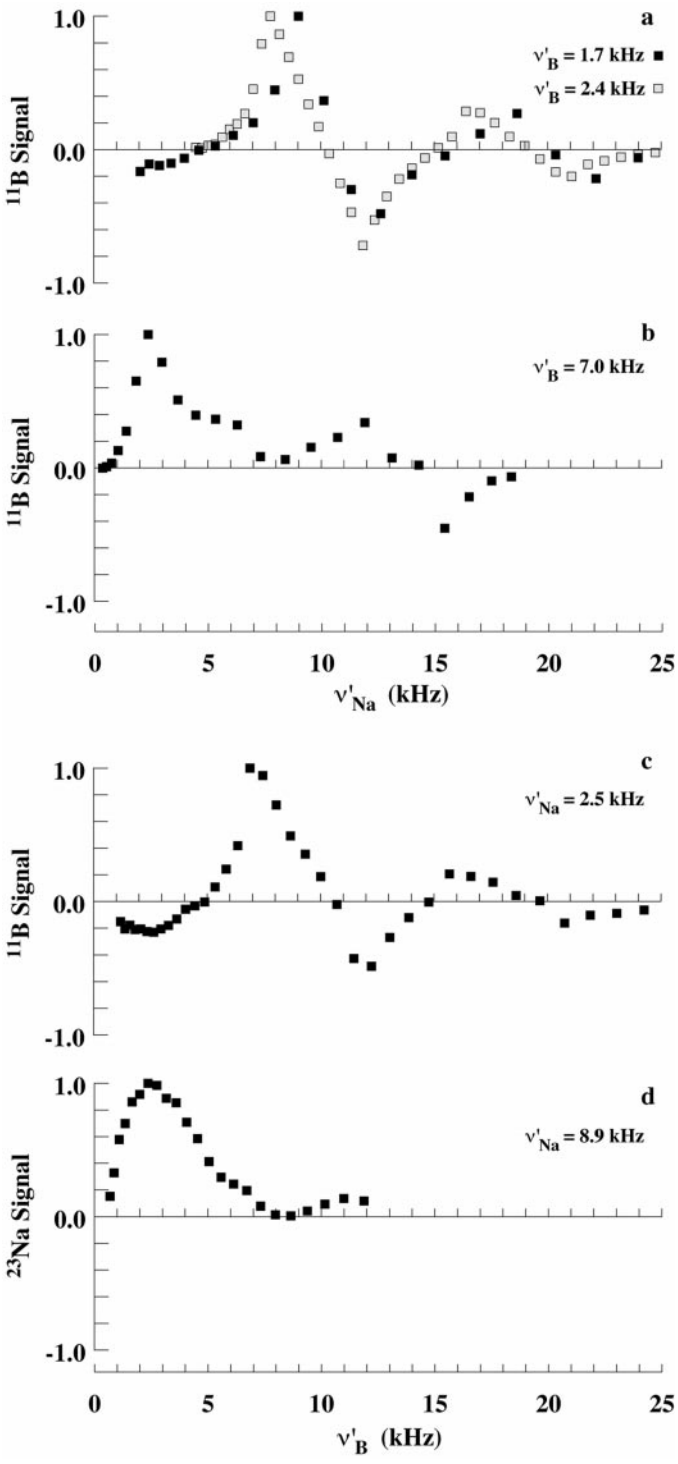

FIG. 5. X → Y CP/MAS spectra of $Na_2B_4O_7$. Pulse delays are given under Experimental. (a) ^{23}Na → ^{11}B, filled squares: ν'_B = 1.7 kHz, 1024 scans, stippled squares: ν'_B = 2.4 kHz, 2048 scans. (b) ^{23}Na → ^{11}B, ν'_B = 7.0 kHz, 1024 scans, 10.0 μs pw_M. (c) ^{23}Na → ^{11}B, ν'_{Na} = 2.5 kHz, 2048 scans. (d) ^{11}B → ^{23}Na, ν'_{Na} = 8.9 kHz, 1536 scans, 20.0 μs pw_M.

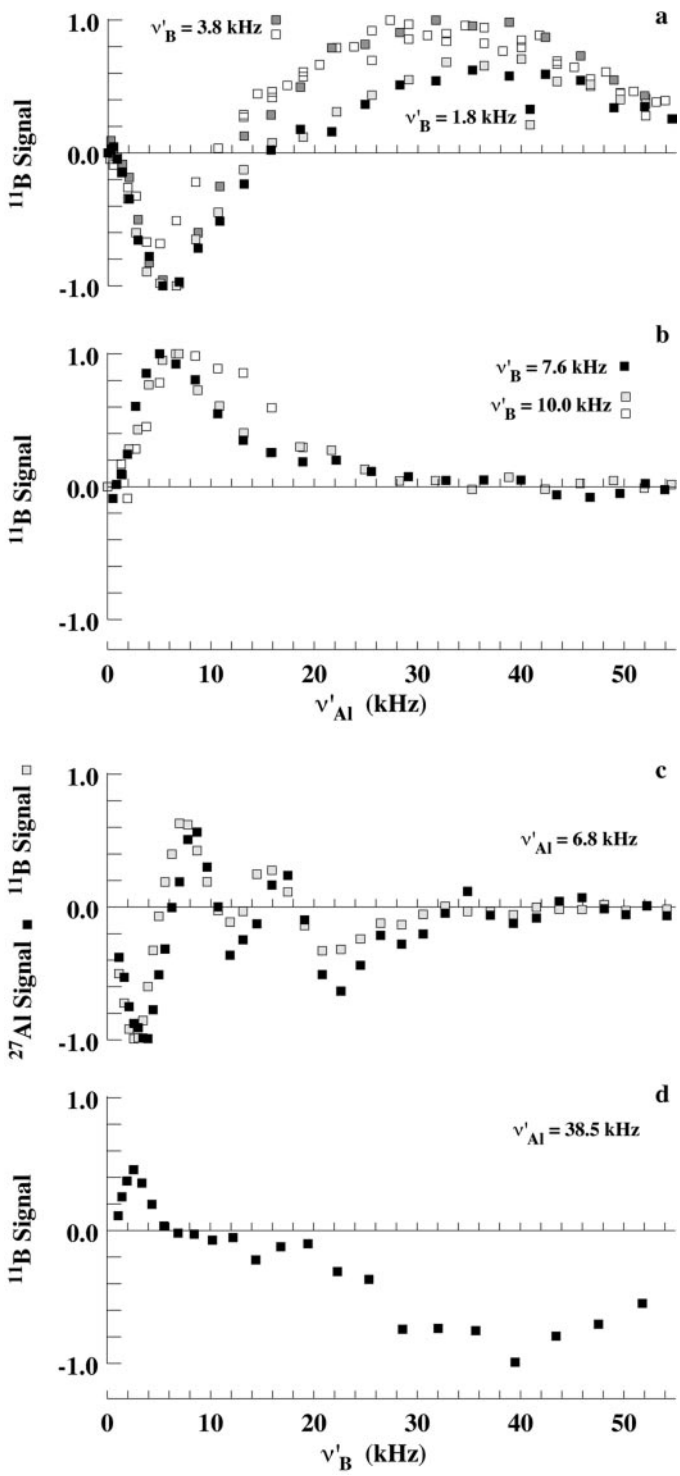

FIG. 6. X → Y CP/MAS spectra of AlB_2. Pulse delays are given under Experimental, except where indicated. (a) ^{27}Al → ^{11}B, 4800 scans, filled and light stippled squares: ν'_B = 1.8 kHz, medium stippled and open squares: ν'_B = 3.8 kHz. (b) ^{27}Al → ^{11}B, 4800 scans, filled squares: ν'_B = 7.6 kHz, stippled and open squares: ν'_B = 10.0 kHz. (c) ν'_{Al} = 6.8 kHz, filled squares: ^{11}B → ^{27}Al, 1024 scans, 4.0 s delay, stippled squares: ^{27}Al → ^{11}B, 4800 scans, 0.5 s delay. (d) ^{27}Al → ^{11}B, 4800 scans, ν'_{Al} = 38.5 kHz.

Paul *et al.* (*11*) presented a plot of intensity of the spin-locked central transition vs radiofrequency field strength for ^{27}Al in albite covering a smaller range of field strengths than

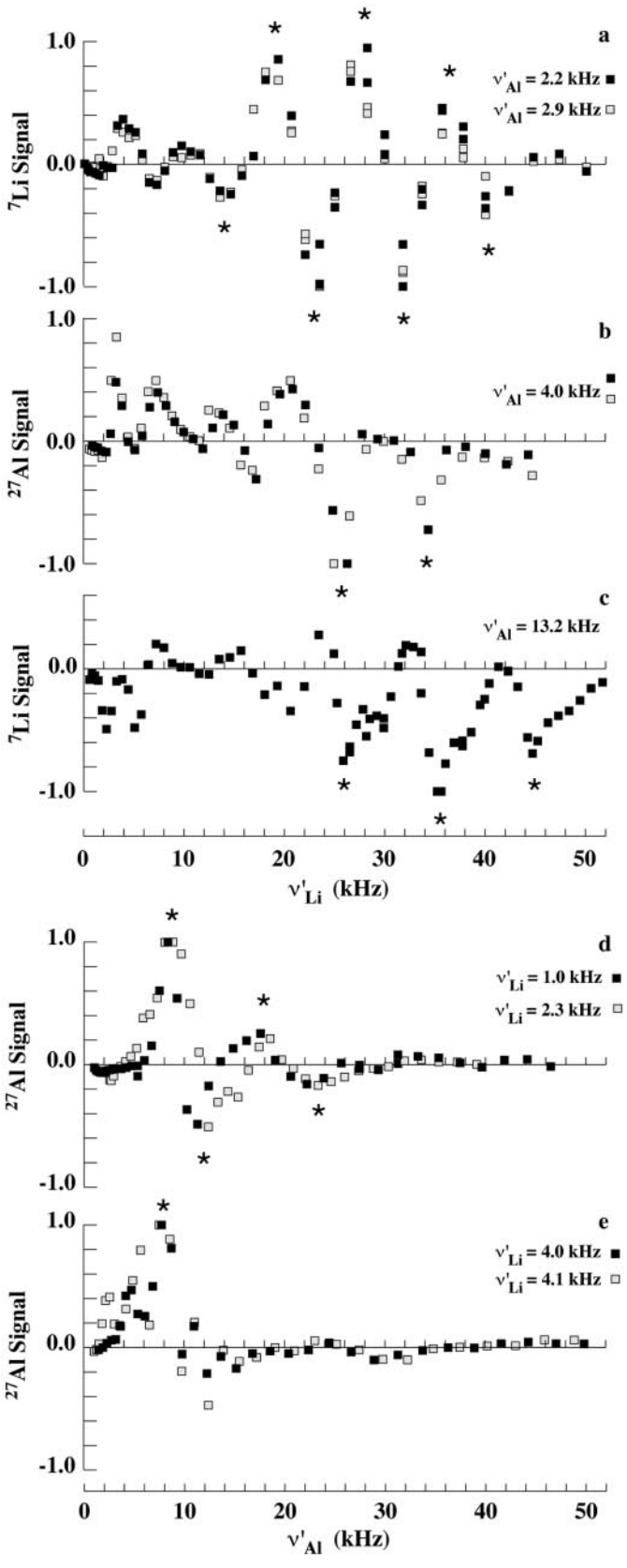

FIG. 7. X → Y CP/MAS spectra of $LiAlO_2$. Pulse delays are given under Experimental. (a) $^{27}Al \rightarrow {}^7Li$, 512 scans, filled squares: $\nu'_{Al} = 2.2$ kHz, stippled squares: $\nu'_{Al} = 2.9$ kHz. (b) $^7Li \rightarrow {}^{27}Al$, 64 scans, filled and stippled squares: $\nu'_{Al} = 4.0$ kHz. (c) $^{27}Al \rightarrow {}^7Li$, 512 scans, $\nu'_{Al} = 13.2$ kHz. (d) $^7Li \rightarrow {}^{27}Al$, 64 scans, filled squares: $\nu'_{Li} = 1.0$ kHz, stippled squares: $\nu'_{Li} = 2.3$ kHz, 8.0 μs pw_M. (e) $^7Li \rightarrow {}^{27}Al$, 64 scans, filled squares: $\nu'_{Li} = 4.0$ kHz, stippled squares: $\nu'_{Li} = 4.1$ kHz.

given here (Figs. 2 and 3). Consistent with their experimental data, these authors present simulations including second-order quadrupolar interactions of the spin-lock efficiency for ^{23}Na and ^{27}Al in albite that have zero intensity at zero field strength and a series of rounded maxima and sharp minima (*11*). The plots of Fig. 3 have the same general form, over which is superimposed one of the two trends noted above, either a general decay as the field strength increases or an intermediate minimum followed by an increase at higher field strengths. Aluminum-27 in aluminum boride has two or three minima (Fig. 3b), and in lithium aluminate has five or six minima (Fig. 3a) between zero and the spinning speed, 10 kHz. (Note that according to Fig. 9 the ν' values for Fig. 3a must be divided by 3 to give the correct field strength, while no correction is required for Fig. 3b).

The spin-locking results presented here uphold the assertion of Sun *et al.* (*20*) that spin-locking efficiency for half-integer quadrupolar nuclei diminishes when the sample spinning frequency and the spin-lock field strength are equal. Although their work involved cases of large quadrupole frequency relative to the spin-lock field strength, our results suggest that this conclusion may apply regardless of the size of ω_Q. Considering Fig. 9, spin-locking fields equivalent to the spinning frequency of 10 kHz occur at ν' values of 20 kHz in Figs. 2a and 2b, 10 kHz and 30 kHz for the ^{27}Al signals of AlB_2 and $LiAlO_2$, respectively, in Fig. 2c, and about 15 kHz in Fig. 2d. All of these are points of relatively low signal on the spin-lock curves.

Evaluation of ϵ_I and ϵ_S in Eqs. [6] and [7] is most reliable for sodium diborate; ϵ_I and ϵ_S are both equal to 2 throughout the range of field strengths used in the CP/MAS experiments, indicating that the quadrupole frequencies are large compared to the radiofrequency field strengths. The expected match conditions are then

$$2\omega_{1B} + 2\omega_{1Na} = n\omega_R, \quad [10]$$

$$2\omega_{1B} - 2\omega_{1Na} = \pm n\omega_R, \quad [11]$$

The first expression agrees with the double-quantum match conditions given by Chan *et al.* (*3*). Figure 9b suggests forms for AlB_2 such as

$$2\omega_{1B} + \omega_{1Al} = n\omega_R, \quad [12]$$

$$2\omega_{1B} - \omega_{1Al} = \pm n\omega_R, \quad [13]$$

but these are not necessarily trustworthy since ^{27}Al may have intermediate rather than small ω_Q as considered above. For

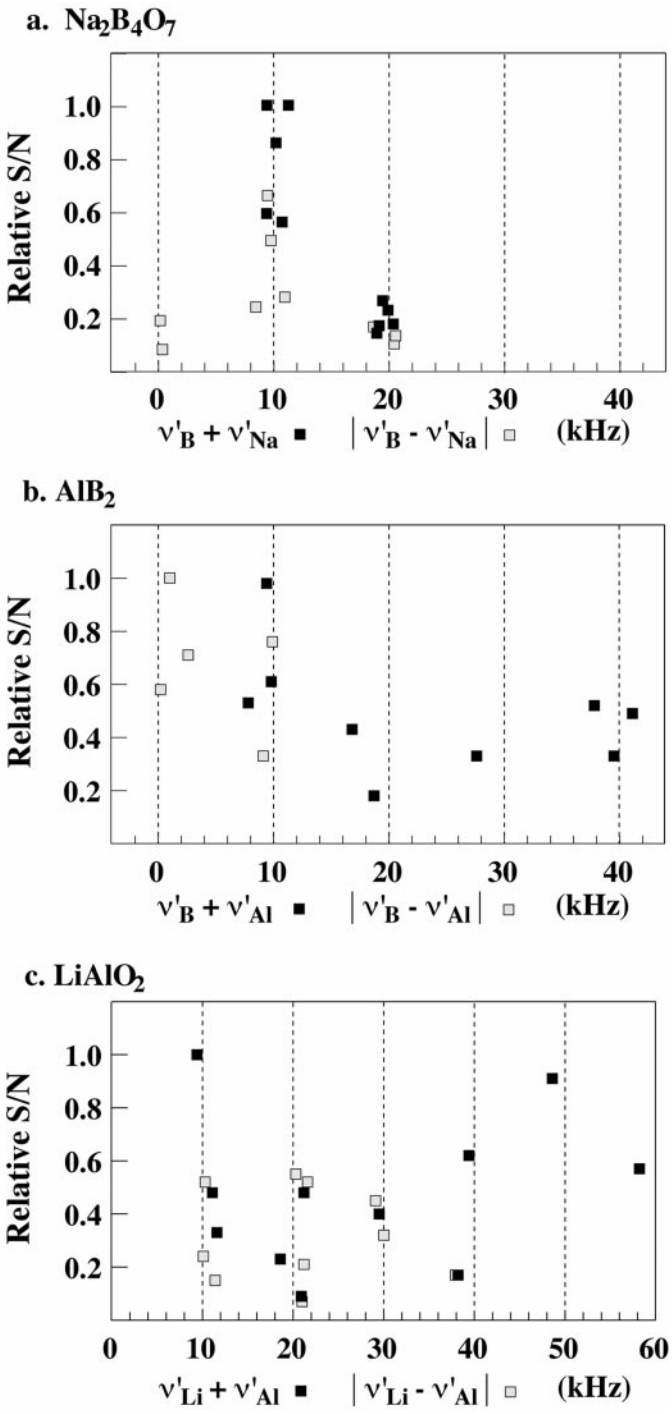

FIG. 8. Relative signal-to-noise vs Hartmann–Hahn match condition (sum or absolute value of the difference of ν' values for the two nuclei) for CP/MAS experiments on (a) $Na_2B_4O_7$, (b) AlB_2, and (c) $LiAlO_2$. Sum (filled squares) and difference (stippled squares) matches were assigned as described in Results. For c, only matches marked with an asterisk in Fig. 7, which are close to integral multiples of the spinning speed, are included. Method of obtaining relative *S*/*N* is explained under Experimental.

$LiAlO_2$ general match conditions are not known due to the apparent intermediate nature of ω_Q of ^{7}Li.

Hartmann–Hahn matches have been assigned here by the assumption that they will be at integral multiples of the spinning frequency of the sample and are expressed in terms of effective nutation frequencies rather than radiofrequency field strengths as in the last paragraph. Examination of Figs. 8a and 9a shows that the assumptions of matches at integral multiples of the spinning frequency and a simple proportionality of the effective nutation frequency and field strength apply quite well to sodium diborate, in which both nuclear species appear to have large quadrupole frequencies in comparison to the radiofrequency field strengths used in CP/MAS. This suggests that the spinning speed of 10 kHz is large enough that the nuclei are in the sudden regime as described by Vega (*8*). These results are similar to those of De Paul *et al.* (*11*) for $^{27}Al \rightarrow {}^{29}Si$ CP/MAS of low albite ($NaAlSi_3O_8$), and to our unpublished $^{23}Na \rightarrow {}^{31}P$ CP/MAS results for $Na_3P_3O_9$, and also agree with the results of Chan *et al.* (*3*) for $^{23}Na \rightarrow {}^{11}B$ CP/MAS of sodium diborate, vindicating the assumption that a simple extension of the match conditions for the $\frac{1}{2} \rightarrow \frac{n}{2}$ case applies to the $\frac{n}{2} \rightarrow \frac{m}{2}$ case where ω_Q is large for both quadrupolar nuclei. The assumption of matches at integral multiples of ν_R may be appropriate for aluminum boride, but matches adhere much less closely to the pattern (Fig. 8b). For lithium aluminate some matches not included in Fig. 8c are clearly inconsistent with this pattern, a result that is not surprising given that ^{7}Li apparently has a quadrupole frequency of intermediate value (Fig. 9c). It should be noted that, even when the familiar match pattern is not followed, there are distinct peaks in the plot of CP/MAS signal vs ν'; showing how these peaks arise from the total aggregate of individual crystallite matches would require a detailed simulation.

A complete theoretical description of $\frac{n}{2} \rightarrow \frac{m}{2}$ CP/MAS taking into account homonuclear dipolar interactions for both types of nuclei has not yet been attempted, but is desirable. One effect of the homonuclear dipolar interactions established for spins $\frac{1}{2}$ is the association of broader Hartmann–Hahn matches with stronger dipolar interactions (*29*). In this work the broadest matches (Figs. 6a and 6d), which may represent overlapping unresolved matches, are observed for aluminum boride. In keeping with this, short distances of about 0.175 nm (*23*) between boron nuclei in AlB_2 imply the strongest dipolar interactions for all nuclei in the samples considered here.

Aluminum boride and lithium aluminate, which appear to have one nuclear species with either small or intermediate ω_Q, have several characteristics in common, but it is not certain how these features are related. Matches with values of *n* greater than 2 are prominent for these samples, unlike for sodium diborate which has large ω_Q for both nuclei. This may relate to the good spin locking of the nuclei with small or intermediate ω_Q and poor spin locking of the nuclei with large ω_Q at the higher powers required for matches with *n* greater than 2. The homonuclear or heteronuclear dipolar interactions that may be the cause of these matches should be significant in all of the samples. A direct connection between the similar spin-locking patterns of ^{27}Al in AlB_2 and ^{7}Li $LiAlO_2$ and the characteristics of variation in the signal sign of each type of

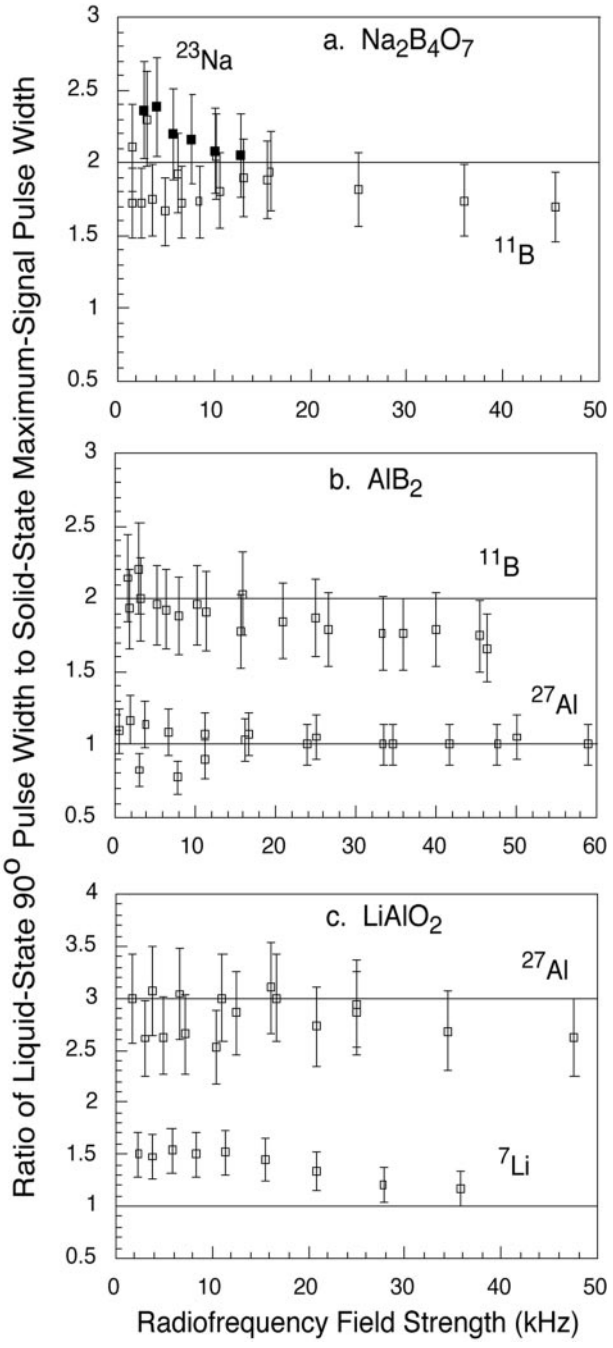

FIG. 9. Correlation of the ratio of the liquid-state 90° pulse width to the solid-state maximum-signal pulse width with the radiofrequency field strength obtained from the liquid-state 90° pulse width, for (a) $Na_2B_4O_7$, (b) AlB_2, and (c) $LiAlO_2$. Liquid samples used are given in Table 1. Error bars assume an error of 10% in each determination of a pulse width.

match (zero- and double-quantum) and deviation from the pattern of matches at integral multiples of the spinning frequency is not clear, but is intriguing. Perhaps the common factor is an intermediate value of ω_Q, despite the apparent contradiction of Fig. 9b.

Figure 8 shows that double-quantum matches for which the two ν' values sum to give the sample spinning frequency are among those having the best signal-to-noise ratio for each of the samples, suggesting that, in samples with at least one nuclear species with large quadrupole frequency, the double-quantum match with n equal to 1 may provide signal comparable to the best achievable. This conclusion may be limited by the crude measure of signal-to-noise given here, the fact that conditions for maximum signal-to-noise such as optimal contact time were not found, and the use of only one spinning speed. Only for $Na_2B_4O_7$ does this first double-quantum match give clearly the best signal-to-noise of all observed; for the other compounds additional match conditions are found that give comparable signal-to-noise.

Two interesting types of complications having to do with lineshapes have been ignored in our treatment of the data. These are distortions of the lineshape known to occur in spin-locking or CP/MAS spectra of half-integer quadrupolar nuclei (*20, 30–32*) and the presence of multiple sites with overlapping resonances. Changes do occur in the lineshapes in the CP/MAS experiments reported here depending upon the radiofrequency field strengths of the contact pulses; these would require better signal-to-noise for a careful analysis. Considering the multiple sites, only one case shows enough resolution to be discussed. This is the case of ^{11}B in sodium diborate (Fig. 4a), for which a distinction can be made between the sharp BO_4 resonance and the broader BO_3 resonance (*3*). The broader signal disappears with increasing field strength for the $n = 2$ matches in Fig. 5c, so that the integral, now smaller because it includes only the sharper signal due to BO_4, gives an incorrect picture of the match position, displacing it to lower field strength. For this reason, these matches were chosen as the maximum of the peak height rather than the maximum of the integral.

CONCLUSIONS

The occurrence of zero-quantum and double-quantum Hartmann–Hahn match conditions with signals of opposite sign has been demonstrated experimentally in $\frac{n}{2} \rightarrow \frac{m}{2}$ CP/MAS of three samples. Double-quantum or sum matches will be evident when the radiofrequency field strengths add up to a multiple of the spinning frequency, which is likely to occur in $\frac{n}{2} \rightarrow \frac{m}{2}$ CP/MAS, for which high spinning speeds and low radiofrequency field strengths are desirable if the quadrupole frequencies are large, and for which matches at greater than two times the spinning frequency involving higher field strengths give substantial signal if one of the nuclei does not have a large quadrupole frequency. The example of sodium diborate shows that $\frac{n}{2} \rightarrow \frac{m}{2}$ CP/MAS between two quadrupolar nuclei with large values of ω_Q relative to the radiofrequency field strength gives matches mainly at one and two times the spinning frequency as expected for $\frac{1}{2} \rightarrow \frac{n}{2}$ CP/MAS in the sudden regime. The examples of lithium aluminate and aluminum boride suggest that if one of the nuclei has intermediate (or small, perhaps for AlB_2) ω_Q the spin-lock pattern as a function of effective nutation frequency for that nucleus has a central minimum,

zero- and double-quantum matches are not consistently of the same sign, and there is only partial adherence to a pattern of matches at integral multiples of the spinning frequency. The size of ω_Q relative to the field strengths used here for ^{27}Al in AlB_2 is in doubt, as our qualitative estimate conflicts with the published value. For the experimental conditions used here, for all samples at least one match of relatively good signal-to-noise in comparison to the others observed is a first double-quantum match for which the effective nutation frequencies add up to the spinning frequency of 10 kHz.

ACKNOWLEDGMENTS

This research was performed at the Oklahoma Statewide Shared NMR Facility, which has been supported by the National Science Foundation (BIR-9512269), the Oklahoma State Regents for Higher Education, the W. M. Keck Foundation, and Conoco Inc. The author acknowledges useful discussions and correspondence with Philip Grandinetti, Antoine Llor, and Karl Mueller.

REFERENCES

1. S. R. Hartmann and E. L. Hahn, Nuclear double resonance in the rotating frame, *Phys. Rev.* **128,** 2042–2053 (1962).
2. L. van Wüllen, L. Züchner, W. Müller-Warmuth, and H. Eckert, ^{11}B{^{27}Al} and ^{27}Al{^{11}B} double-resonance experiments on a glassy sodium aluminoborate, *Solid State Nucl. Magn. Reson.* **6,** 203–212 (1996).
3. J. C. C. Chan, M. Bertmer, and H. Eckert, Double-quantum cross-polarization between half-integer quadrupolar spin systems: ^{11}B ↔ ^{23}Na and ^{11}B ↔ ^{27}Al, *Chem. Phys. Lett.* **292,** 154–160 (1998).
4. A. Medek, J. S. Harwood, and L. Frydman, Multiple-quantum magic-angle spinning NMR: A new method for the study of quadrupolar nuclei in solids, *J. Am. Chem. Soc.* **117,** 12779–12787 (1995).
5. S. H. Wang, S. M. De Paul, and L. M. Bull, High-resolution heteronuclear correlation between quadrupolar and spin-$\frac{1}{2}$ nuclei using multiple-quantum magic-angle spinning, *J. Magn. Reson.* **125,** 364–368 (1997).
6. C. A. Fyfe, K. T. Mueller, H. Grondey, and K. C. Wong-Moon, Solid-state double-resonance NMR experiments involving quadrupolar and spin $\frac{1}{2}$ nuclei, *J. Phys. Chem.* **97,** 13484–13495 (1993).
7. A. J. Vega, MAS NMR spin locking of half-integer quadrupolar nuclei, *J. Magn. Reson.* **96,** 50–68 (1992).
8. A. J. Vega, CP/MAS of quadrupolar S = $\frac{3}{2}$ nuclei, *Solid State Nucl. Magn. Reson.* **1,** 17–32 (1992).
9. A. Abragam, "Principles of Nuclear Magnetism," Oxford Univ. Press, Oxford (1961).
10. B. H. Meier, Cross polarization under fast magic angle spinning: Thermodynamical considerations, *Chem. Phys. Lett.* **188,** 201–207 (1992).
11. S. M. De Paul, M. Ernst, J. S. Shore, J. F. Stebbins, and A. Pines, Cross-polarization from quadrupolar nuclei to silicon using low-radio-frequency amplitudes during magic-angle spinning, *J. Phys. Chem. B* **101,** 3240–3249 (1997).
12. E. O. Stejskal, J. Schaefer, and J. S. Waugh, Magic-angle spinning and polarization transfer in proton-enhanced NMR, *J. Magn. Reson.* **28,** 105–112 (1977).
13. D. Freude and J. Haase, Quadrupole effects in solid-state nuclear magnetic resonance, *in* "NMR Basic Principles and Progress, Volume 29," Springer-Verlag, Berlin (1993).
14. M. M. Maricq and J. S. Waugh, NMR in rotating solids, *J. Chem. Phys.* **70,** 3300–3316 (1979).
15. A. Samoson and E. Lippmaa, Excitation phenomena and line intensities in high-resolution NMR powder spectra of half-integer quadrupolar nuclei, *Phys. Rev. B* **28,** 6567–6570 (1983).
16. A. P. M. Kentgens, J. J. M. Lemmens, F. M. M. Geurts, and W. S. Veeman, Two-dimensional solid-state nutation NMR of half-integer quadrupolar nuclei, *J. Magn. Reson.* **71,** 62–74 (1987).
17. J. C. Edwards and P. D. Ellis, Cross-polarization for quadrupolar nuclei—Proton to molybdenum-95, *Magn. Reson. Chem.* **28,** S59–S67 (1990).
18. P. P. Man, J. Klinowski, A. Trokiner, H. Zanni, and P. Papon, Selective and non-selective NMR excitation of quadrupolar nuclei in the solid state, *Chem. Phys. Lett.* **151,** 143–150 (1988).
19. D. Marks and S. Vega, A theory for cross-polarization NMR of nonspinning and spinning samples, *J. Magn. Reson. A* **118,** 157–172 (1996).
20. W. Sun, J. T. Stephen, L. D. Potter, and Y. Wu, Rotation-induced resonance and second-order quadrupolar effects on spin locking of half-integer quadrupolar nuclei, *J. Magn. Reson. A* **116,** 181–188 (1995).
21. G. Jeschke, Spin locking of I = $\frac{3}{2}$ nuclei in static and spinning samples: A description by abstract spins and Floquet formalism, *J. Chem. Phys.* **108**(3), 907–917 (1998).
22. J. Krogh-Moe, The crystal structure of sodium diborate $Na_2O \cdot 2B_2O_3$, *Acta Crystallogr.* **B30,** 578–582 (1974).
23. B. Aronsson, T. Lundström, and S. Rundqvist, "Borides, Silicides and Phosphides," Methuen, London (1965).
24. M. Marezio, The crystal structure and anomalous dispersion of γ-$LiAlO_2$, *Acta Crystallogr.* **19,** 396–400 (1965).
25. A. Pines, M. G. Gibby, and J. S. Waugh, Proton-enhanced NMR of dilute spins in solids, *J. Chem. Phys.* **59,** 569–590 (1973).
26. J. P. Kopp and R. G. Barnes, Nuclear magnetic resonance of ^{11}B and ^{27}Al in aluminum diboride, *J. Chem. Phys.* **54,** 1840–1841 (1971).
27. D. Müller, W. Gessner, and G. Scheler, Chemical shift and quadrupole coupling of the ^{27}Al spectra of $LiAlO_2$ polymorths, *Polyhedron* **2,** 1195–1198 (1983).
28. E. Sirtl and L. M. Woerner, Preparation and properties of aluminum diboride single crystals, *J. Cryst. Growth* **16,** 215–218 (1972).
29. M. H. Levitt, D. Suter, and R. R. Ernst, Spin dynamics and thermodynamics in solid-state NMR cross polarization, *J. Chem. Phys.* **84,** 4243–4255 (1986).
30. S. Hayashi, Magic-angle spinning magnetic resonance of half-integer quadrupole nuclei: Effect of spin-locking efficiency on powder lineshapes, *Solid State Nucl. Magn. Reson.* **3,** 93–101 (1994).
31. S. Ding and C. A. McDowell, Theoretical calculations of the CPMAS spectral lineshapes of half-integer quadrupole systems, *J. Magn. Reson. A* **114,** 80–87 (1995).
32. S. Ding and C. A. McDowell, Spin-locking spectral lineshapes of the central transition of half-integer quadrupole systems under magic-angle spinning, *J. Mol. Struct.* **355,** 135–142 (1995).